Inelastic collisions in molecular oxygen at low temperature ($4 \leq T \leq 34$ K). Close-coupling calculations versus experiment

J. Pérez-Ríos,[1] G. Tejeda,[2] J. M. Fernández,[2] M. I. Hernández,[1] and S. Montero[2,a)]
[1]*Instituto de Física Fundamental, CSIC Serrano 123, 28006 Madrid, Spain*
[2]*Laboratory of Molecular Fluid Dynamics, Instituto de Estructura de la Materia, CSIC Serrano 121, 28006 Madrid, Spain*

(Received 23 February 2011; accepted 5 April 2011; published online 3 May 2011)

Close-coupling calculations and experiment are combined in this work, which is aimed at establishing a set of state-to-state rate coefficients for elementary processes $ij \rightarrow \ell m$ in O_2:O_2 collisions at low temperature involving the rotational states i, j, ℓ, m of the vibrational ground state of $^{16}O_2(^3\Sigma_g^-)$. First, a set of cross sections for inelastic collisions is calculated as a function of the collision energy at the converged close-coupled level via the MOLSCAT code, using a recent *ab-initio* potential energy surface for O_2-O_2 [M. Bartolomei *et al.*, J. Chem. Phys. **133**, 124311 (2010)]. Then, the corresponding rates for the temperature range $4 \leq T \leq 34$ K are derived from the cross sections. The link between theory and experiment is a Master Equation which accounts for the time evolution of rotational populations in a reference volume of gas in terms of the collision rates. This Master Equation provides a linear function of the rates for each rotational state and temperature. In the experiment, the evolution of rotational populations is measured by Raman spectroscopy in a tiny reference volume ($\approx 2 \times 10^{-4}$ mm^3) of O_2 travelling along the axis of a supersonic jet at a velocity of $\approx$700 m/s. The accuracy of the calculated rates is assessed experimentally for $10 \leq T \leq 34$ K by means of the Master Equation. The rates, jointly with their confidence interval estimated by Monte Carlo simulation, account to within the experimental uncertainty for the evolution of the populations of the $N = 1, 3, 5, 7$ rotational triads along the supersonic jet. Confidence intervals range from $\approx$6% for the dominant rates at 34 K, up to $\approx$17% at 10 K. These results provide an experimental validation of state-to-state rates for O_2:O_2 inelastic collisions calculated in the close-coupling approach and, indirectly, of the anisotropy of the O_2-O_2 intermolecular potential employed in the calculation for energies up to 300 cm^{-1}. © *2011 American Institute of Physics*. [doi:10.1063/1.3585978]

I. INTRODUCTION

Rotational excitation and de-excitation of molecules by inelastic collisions with atoms or other molecules is a problem of increasing importance in the physics and chemistry of rarefied gases. Modeling of media such as the interstellar molecular gas, planetary atmospheres, comet environments, or laboratory supersonic jets and molecular beams requires a deep knowledge of inelastic collisions in the lower end of the thermal scale. But also remote probing of such media rests upon inelastic collisions, since all detection methods based on spectral line shapes and widths depend quantitatively on the collision scattering matrix.[1] This matrix can be calculated accurately by solving the close-coupling Schrödinger equations[2] provided a good potential energy surface (PES) for the interacting molecules is available. The information associated to the molecular collisions involving (i, j) precollisional and (ℓ, m) post-collisional quantum states is usually expressed in terms of the kinetic energy of the collision by means of the state-to-state cross sections $\sigma_{ij\rightarrow\ell m}$ or, more commonly, in terms of the translational temperature of the gas medium by means of the related rate coefficients $k_{ij\rightarrow\ell m}$. In any case the procedure implies a high computational cost.

As stated by the generalized Boltzmann equation, the $\sigma_{ij\rightarrow\ell m}$'s, or their associated $k_{ij\rightarrow\ell m}$ rates, quantify the effect of elementary collisional events $ij \rightarrow \ell m$ onto the time-space evolution of the position(r)-velocity(v) distribution function.[3–6] A central result of these developments is the mathematical theory of transport phenomena.[7–10] Nonetheless, the experimental and theoretical information available so far on the main transport properties of O_2 (shear and volume viscosity, thermal conductivity, diffusion coefficient, etc.) is very limited at temperatures under 300 K. Molecular dynamics simulations of these quantities have been reported for the thermal range between $200 < T < 600$ K, showing a modest agreement with the experiment.[11]

Spectral lineshape studies on pure O_2 spanning the thermal domain from 100 up to 1600 K have been reported for several spectral regions employing different approaches. Microwave and Raman spectral line shapes, and relaxation effects were studied in connection with an empirical potential for $O_2 + O_2$.[12] Self-broadening, shifting, and line-mixing coefficients for pure O_2 have been investigated in the A-band region by Fourier-transform absorption spectroscopy in the visible ($\approx$13000 cm^{-1}),[13] in the 60-GHz and 118-GHz bands ($\approx$2 and $\approx$4 cm^{-1}) by microwave spectroscopy,[14,15] in the fundamental vibration-rotation band by coherent anti-Stokes Raman spectroscopy[16] and stimulated Raman spectroscopy,[17,18] and in the pure rotational spectral region (0–150 cm^{-1}) by

a)Author to whom correspondence should be addressed. Electronic mail: em-salvador@iem.cfmac.csic.es.

spontaneous Raman spectroscopy.[19] Other works on spectral lineshapes of O_2 in air can be found in the literature.[20–22] The interpretation of many of these data has been conducted within approximated semiclassical collisional models. However, as far as we are aware, the problem has not been considered yet in terms of the exact quantum scattering theory using state-to-state collisional cross sections or rates.

The aforementioned reasons point at the central role of cross sections and rates for studying today's fundamental problems, and practical problems tomorrow. Aquilanti *et al.*[23] measured total integral cross sections of rotationally hot and cold molecular beams of molecular O_2 by target O_2 and derived an intermolecular PES from these data.[24] They were not able, however, to obtain information about state-to-state rotationally inelastic processes, which are highly sensitive to the anisotropy of the interaction. Scattering calculations have provided some preliminary results on de-excitation rates of oxygen molecules by inelastic collision with helium atoms,[25–28] as well as on O_2:O_2 self-collisions.[29] However, no experimental data on the subject appear to have been reported to date.

In the present work we report a computational-experimental study where the relevant set of rates for O_2:O_2 inelastic collisions in the thermal range $4 \leq T \leq 34$ K is calculated in the frame of the close-coupling method[2,30] using a recent global *ab-initio* PES for the O_2-O_2 interactions.[31] This PES represents a considerable improvement with respect to previous *ab-initio* potentials[32,33] mainly because electronic correlation is included by means of high level methods. The accuracy of the calculated rates is then assessed experimentally in the range $10 \leq T \leq 34$ K by means of the evolution of rotational populations measured by Raman spectroscopy along supersonic jets of pure O_2. The confidence interval of the rates is obtained by a comparison with the experimental data, in this way validating quantitatively the PES employed in the close-coupling calculation.

II. CLOSE-COUPLING CALCULATIONS

A. Energy levels of O_2

The $^{16}O_2$ molecule considered here in its $^3\Sigma_g^-$ electronic ground state has total electron spin $S = 1$, which arises from the parallel spins of its two unpaired electrons. Coupling of the total electron spin with the rotational angular momentum N (Hund's case **b**) leads to a total angular momentum vector $\mathbf{J} = \mathbf{S} + \mathbf{N}$. Consequently, the possible values of the total angular momentum quantum number for the rotational levels are $J = N, N \pm 1$, with $N = 1, 3, 5, \ldots$. For each N, the rotational levels are grouped in triads $J = N + 1$, $J = N$, and $J = N - 1$, shown in Fig. 1. Raman-active (Stokes) transitions between these levels obey $\Delta N = +2$ and $\Delta J = 0, +1, +2$ selection rules. Some of these six active ΔJ transitions differ by less than 0.1 cm^{-1} and cannot be resolved by the linear Raman spectroscopy set up employed in this work, with the result that just a triplet is observed for each $N \rightarrow N + 2$ band. These triplets (see Fig. 1, bottom) display an intense central band and two satellites at $\approx \pm 2$ cm^{-1} from it, which decrease fast in intensity for an increasing N. Since the rotational temperature in the present experiments is $T_r \geq 19$ K and the spectral resolution is ≈ 0.5 cm^{-1}, the transfer of population induced by

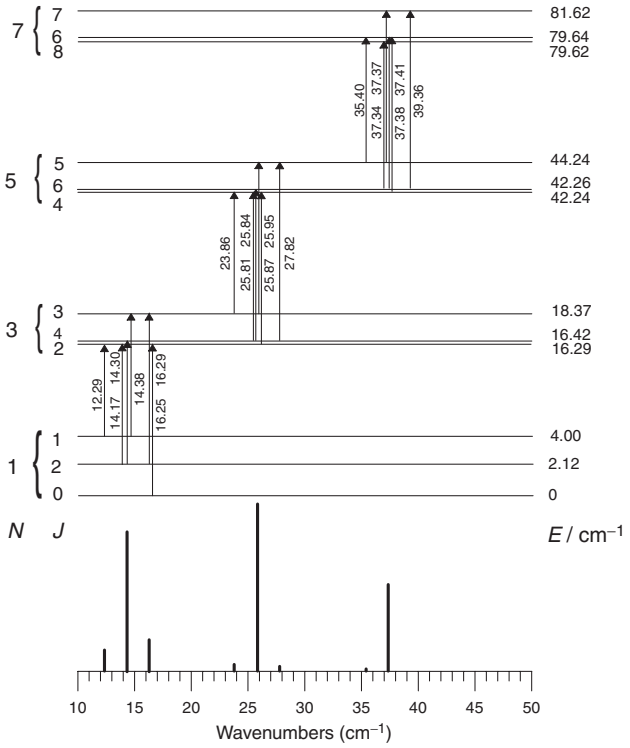

FIG. 1. Structure of the $N \rightarrow N + 2$ triplets in the rotational Raman spectrum of $^{16}O_2$. Adapted from Ref. 19.

$$O_2(N_a, J_a) + O_2(N_b, J_b) \longrightarrow O_2(N'_a, J'_a) + O_2(N'_b, J'_b), \quad (1)$$

elementary collisional processes between the resolved N, J levels of molecules a and b is hardly detectable, and only global transfer between N-triads can be measured with the required accuracy. This is described by the reduced process,

$$O_2(N_a) + O_2(N_b) \longrightarrow O_2(N'_a) + O_2(N'_b), \quad (2)$$

which will be generically described below as

$$O_2(i) + O_2(j) \longrightarrow O_2(l) + O_2(m), \quad (3)$$

by means of reduced cross sections $\sigma_{ij \rightarrow lm}$ in terms of energy of the colliding pairs, or by reduced rates $k_{ij \rightarrow lm}$ in terms of the translational temperature of the thermal bath. This simplification implies that all collisions where $N_a = N'_a$ and $N_b = N'_b$ or $N_a = N'_b$ and $N_b = N'_a$ are considered as elastic, whatever the ΔJ changes occurring in the collision.

B. Potential energy surface of $O_2 + O_2$, inelastic cross sections, and rates

The open-shell character of $O_2(^3\Sigma_g^-)$ implies that the $O_2 + O_2$ collision complex may have total electron spin 0, 1, or 2, with singlet, triplet, or quintet spin multiplicity, respectively. In this work we have used a recent *ab-initio* PES where the quintet multiplicity was obtained by the restricted coupled cluster with single, double, and perturbative triple excitations [RCCSD(T)] method,[34] whereas the singlet

and triplet PES's referred as CC-PT2 in Ref. 31 were obtained by combining the RCCSD(T) quintet potential with calculations of the singlet-quintet and triplet-quintet splittings at the complete active space second order perturbation (CASPT2) level of theory. Due to the anisotropy of the interaction, spherical harmonic expansions with a large number of terms were built from the *ab-initio* data. These PES's were extended for large intermolecular distances by using *ab-initio* long range coefficients.[35] The new *ab-initio* PES's provide fairly good agreement with experimental second virial coefficients,[31] as well as with the glory structures of total cross sections in molecular beam experiments.[24] Such experimental data largely yield information on the isotropic part of the PES's, and only to some extent on its anisotropy. In contrast, the present collision experiments provide significant information on the anisotropy of the PES's.

The theory for the calculation of the $\sigma_{ij\to lm}$ cross sections in the scattering of two identical linear rigid rotors has been reviewed recently.[29] Here we focus on some aspects specifically related to the present problem and refer to Ref. 29 for details, particularly those regarding the indistinguishability of the colliding partners.

The molecular symmetry group for the interaction between two identical homonuclear diatoms is G_{16}.[29,36] In the MOLSCAT code,[30] used in this work, the close-coupled equations were solved separately for each symmetry block of G_{16}.[37] Appropriate statistical weights have been given to the computed symmetry-adapted cross sections.[29] Regarding the monomers exchange operation, the singlet and quintet electronic states of $O_2 + O_2$ are symmetric, whereas the triplet one is antisymmetric.[38] Therefore, the cross sections must be obtained using even ($\xi = +1$) or odd ($\xi = -1$) spatial wave functions for the singlet (S) and quintet (Q), or triplet (T) states, respectively,

$$\sigma_{ij\to lm}^{S,T,Q} \equiv \sigma_{ij\to lm}^{ind,\xi} \quad \begin{matrix} \xi = +1, & \text{S, Q states} \\ \xi = -1, & \text{T state} \end{matrix}, \tag{4}$$

where $\sigma_{ij\to lm}^{ind,\xi}$ refers to the cross section for indistinguishable molecules.

In order to determine the adequate correction factors for preventing double counting when the rotational states of reactants/products are the same ($i = j$ and/or $l = m$), it is useful to recall the relationship between the cross sections for distinguishable and indistinguishable molecules:[29,37]

$$\sigma_{ij\to lm}^{ind,\xi} = \sigma_{ij\to lm}^{d} + \sigma_{ij\to ml}^{e} + \xi\sigma_{ij\to lm}^{int}, \tag{5}$$

where σ^d and σ^e refer to the so-called direct and exchange processes,[39] and $\sigma_{ij\to lm}^{int}$ accounts for quantum interference effects. Neglecting such interference effects, Eq. (5) is the same as Eq. (29) of Ref. 40, except for a correction factor

$$F_1 = (1 + \delta_{ij}\delta_{lm})[(1 + \delta_{ij})(1 + \delta_{lm})]^{-1}. \tag{6}$$

There is no agreement in the literature about this factor, as a different factor

$$F_2 = [(1 + \delta_{ij})(1 + \delta_{lm})]^{-1}, \tag{7}$$

has been employed by other authors.[41–44] The difference between F_1 and F_2 only affects those cross sections and rates where $i = j$ and $\ell = m$, becoming $F_2 = F_1/2$ for these cases. The experimental results discussed in this work provide some clues about these factors. Unless otherwise indicated, the results given below have been calculated with F_2.

The calculated singlet, triplet, and quintet cross sections differ from each other by up to 20%. In order to compare with the experiment they have been averaged using the degeneracy of each PES as statistical weight.[24] In summary, the cross sections to be used in the calculation of the rate coefficients are given by

$$\sigma_{ij\to lm} = F_\alpha \times \frac{5\sigma_{ij\to lm}^{Q} + 3\sigma_{ij\to lm}^{T} + \sigma_{ij\to lm}^{S}}{9}, \tag{8}$$

with $\alpha = 1$ or 2.

The rate coefficients are then obtained by the transformation

$$k_{ij\to lm}(T_t) = \frac{\langle v\rangle}{(k_B T_t)^2}\int_{E_s}^{\infty} \frac{\sigma_{ij\to lm}(E)}{\exp(E/k_B T_t)} E dE, \tag{9}$$

which averages the cross sections weighted with the Boltzmann distribution over a range of energies. This leads to a smooth dependence of the $k_{ij\to lm}$ rates on the translational temperature (T_t); $E = E_T - E_i - E_j$ is the available precollisional kinetic energy for the molecules in the i and j rotational levels, E_s is the minimum kinetic energy for the rotational levels l and m to become accessible, and $\langle v\rangle = (8k_B T_t/\pi\mu)^{1/2}$ is the mean relative velocity of the colliding partners of reduced mass μ for a Boltzmann distribution.

C. Computational details and results

The MOLSCAT code[30] has been used for computing the cross sections for the singlet, triplet, and quintet PES's of Ref. 31. The cross sections were computed with the symmetry ξ according to Eq. (4), and the quantum interference effects included in Eq. (5) were found to be negligible at most energies. Such effects become completely washed out in the calculation of the rate coefficients.

A total of 16 pairs of rotational levels of $^{16}O_2$ were included in the close-coupled equations. Their internal energies are listed in Table A1 of the supplementary material.[45] The calculations were carried out for a grid of 700 points ranging from a total energy $E_T = 20.13$ cm^{-1} up to 300 cm^{-1}. The energy step was of 1 cm^{-1} in the regions with small $d\sigma/dE_T$ gradients, decreasing the step size to 0.3 cm^{-1} for increasing gradients. Even denser grids were employed near the opening of the different channels in order to account for converged rate coefficients at the lowest translational temperatures. The close-coupled equations were solved by means of the hybrid log-derivative-Airy propagator of Alexander and Manolopoulos.[46] The propagation was carried out with the modified log-derivative method from a minimum intermolecular distance of 2.5 Å to an intermediate one of 11.7 Å, and with the Airy method up to a maximum of 27.3 Å. Typical step sizes for the log-derivative propagation were about 0.03 Å. The reduced mass used was 15.9949146 amu. Total angular momentum $\mathcal{J}$ of the collision complex was increased until the partial cross sections for the last four consecutive

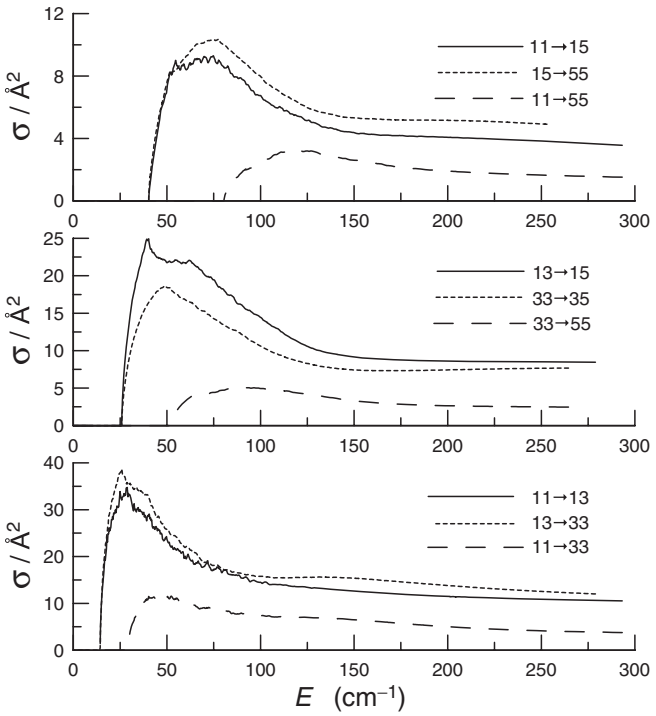

FIG. 2. Close-coupling calculated excitation state-to-state cross sections for O_2:O_2 collisions versus the available precollisional kinetic energy (E). Factor F_2 employed in the calculation. Colliding molecules considered indistinguishable.

$\mathcal{J}$'s contributed each with less than 0.005 Å^2 (this led to a maximum of $\mathcal{J} = 126$ for the highest energy considered).

Convergence of the close-coupling calculations with the number of channels is slow. In order to check the convergence of the cross sections with the rotational basis, test calculations at given values of the total energy have been run including six additional pairs of rotational levels. The results are shown in Table A2.[45] These calculations imply solving sets of close-coupling equations of about 800 and 1500 channels, respectively, for each value of $\mathcal{J}$. As shown in Table A2,[45] the cross sections for the lowest energies (≈100 cm^{-1}) are converged to better than 1%, whereas for the highest energy (≈300 cm^{-1}) some errors become ≈10%. However, these poorly converged cross-sections have little impact in the context of the Master Equation (MEQ) considered below, since they are multiplied in Eq. (9) by the tail of the Boltzmann distribution when transformed into rate coefficients. Such tails are small in the thermal range investigated here.

The calculated set of cross sections includes most collisionally induced transitions in the domain of quantum number $N = \{i, j, \ell, m\} \leq 9$, ($N = odd$) and reduced energy gaps

$$\Delta/B = |i(i+1) + j(j+1) - \ell(\ell+1) - m(m+1)| \leq 108,$$

where $B = 1.43767$ cm^{-1} is the rotational constant of $^{16}O_2$.[47] A representative set of calculated cross sections is shown in Fig. 2.

The rate coefficients were obtained from a numerical integration of Eq. (9). For the range of energies used in the calculation of the cross sections, the convergence of the rate coefficients is guaranteed to better than 5% for translational temperatures 4K ≤ T_t ≤ 34 K. A selection of rates for the collisional transitions between the lowest N-triads is given in Table I. A larger set including 66 processes is given in Table A3.[45] This set is complete enough to discuss the experimental results up to 34 K without omitting significant collisional contributions.

TABLE I. A selection of close-coupling calculated down-rate coefficients $k_{ij\to\ell m}$ for O_2:O_2 collision-induced transitions between the lowest rotational N-triads of O_2 at 34, 22, and 10 K; Δ/B are the reduced energy gaps (see text); 1σ confidence intervals with respect to the experiment are given. Rates are in units of 10^{-20} m^3/s. Colliding molecules are considered indistinguishable. See extended Table A3 in Ref. 45.

Process $ij \to \ell m$	Δ/B	T_t = 34 K	22 K	10 K
51 → 33	8	5020	5351	5477
		±650	±368	±1456
31 → 11	10	3422	3621	3755
		±334	±267	±626
33 → 13	10	3824	4060	4218
		±241	±236	±753
35 → 15	10	4654	4728	4557
		±380	±535	±3122
37 → 17	10	3141	3075	2922
		±1056	±2411	a
39 → 19	10	2320	2217	2050
		a	a	a
15 → 13	18	5221	5475	5478
		±544	±278	±1951
53 → 33	18	3843	3941	3709
		±392	±240	±2317
55 → 35	18	3460	3544	3472
		±615	±548	a
57 → 37	18	4824	4838	4546
		±1761	±2843	a
33 → 11	20	770	806	826
		±62	±65	±277
51 → 11	28	1086	1132	1077
		±206	±201	<2800
53 → 13	28	2875	2948	2788
		±149	±171	±2070
55 → 15	28	1206	1242	1179
		±229	±394	a
57 → 17	28	1742	1804	1752
		±651	±1801	a

[a]a=ill-determined

III. MASTER EQUATION

The link between experiment (the jet axis) and theory (the calculated collisional rates) is provided by a MEQ: (Ref. 40)

$$\frac{dP_i}{dt} = n \sum_j \sum_{\ell \leq m} (-P_i P_j k_{ij\to\ell m} + P_\ell P_m k_{\ell m \to ij}) Q_{ij\ell m}, \tag{10}$$

which describes the time evolution of the population P_i of a quantum state i as a consequence of inelastic collisions in a single-component molecular gas at instantaneous number density n and translational temperature T_t. In the absence of chemical reactions or radiative transfer the MEQ (10)

represents the conservation of matter, and is free from approximations other than neglecting triple collisions. These conditions are satisfied in the experiments described below.

The indices i, j, ℓ, m in Eq. (10) are to be identified here with the rotational quantum number N of the colliding O_2 molecules, and the $k_{ij\to\ell m}$'s with the inelastic collisional rates at the local translational temperature $T_t(z)$ involved in the reduced processes of Eqs. (2) and (3) occurring at position z of the jet axis. This means that P_i is the population of the rotational triad of close-lying energy levels for $i = N$, with the normalization $\Sigma_N P_N = 1$.

The collisional medium where Eq. (10) is applied to is a tiny parcel of gas at instantaneous distance z from the nozzle and translational temperature $T_t(z)$, travelling along the jet axis with supersonic flow velocity $V(z) = dz/dt$. The $^{16}O_2$ molecules involved in the O_2:O_2 collisions within the travelling gas parcel are considered indistinguishable, with the factor

$$Q_{ij\ell m} = [1 + \delta_{ij}(1 - \delta_{\ell i})(1 - \delta_{mi})] \times [1 - \delta_{\ell i}(1 - \delta_{ij})][1 - \delta_{mi}(1 - \delta_{ij})], \quad (11)$$

accounting in MEQ (10) for the symmetry effects in collisions between indistinguishable molecules.[40]

The rates defined by Eq. (9) obey the detailed balance:

$$k_{\ell m\to ij} = k_{ij\to\ell m}\frac{(2i+1)(2j+1)}{(2\ell+1)(2m+1)} \times e^{(E_\ell+E_m-E_i-E_j)/k_BT_t}, \quad (12)$$

where E_i, E_j, E_ℓ, E_m are the energies of the rotational N-triads involved. The upward ("up") and downward ("down") rates will, henceforth, be labeled as $k^{up}_{ij\to\ell m}$ and $k^{down}_{\ell m\to ij}$, respectively, under the constraint $E_i + E_j < E_\ell + E_m$.

Since "up" and "down" rate coefficients may differ at low temperature by many orders of magnitude, it is convenient to reformulate the MEQ (10) in terms of only "down" rates, which shows a far smoother thermal dependence than the "up" rates. With aid of Eq. (12), the MEQ (10) can then be rewritten in the general form,

$$dP_i/dt = \sum_{\tau\omega\sigma\rho} a_{\tau\omega\sigma\rho}k^{down}_{\tau\omega\to\sigma\rho}, \quad (13)$$

in terms of only "down"rates, i.e., with rotational energy $E_\tau + E_\omega > E_\sigma + E_\rho$. The indices $\tau, \omega, \sigma, \rho$ run over the values of the rotational quantum number N, and at least one of these indices must be equal to i.

The left-hand-side (LH-side) of MEQ (13) accounts for the population rates dP_i/dt of the rotational triads $i = N$. It is fully determined by the local experimental quantities $P_i(z)$ and $T_t(z)$ along the jet. In turn, each $a_{\tau\omega\sigma\rho}k^{down}_{\tau\omega\to\sigma\rho}$ term in the right-hand side (RH-side) of MEQ (13) accounts in a convenient factorized form (instantaneous local quantities × intermolecular properties) for the net contribution of the $\sigma\rho \to \tau\omega$ and $\tau\omega \to \sigma\rho$ time-symmetric collisional processes to the population rate dP_i/dt. Coefficients $a_{\tau\omega\sigma\rho}$ are determined by the experimental data $n(z)$, $P_i(z)$, and $T_t(z)$, and have been calculated with MEQO2.FOR (option 1), an ad hoc FORTRAN code. The quantities n, P_i, and T_t have been measured as described in detail in Sec. IV.

The $k^{down}_{\tau\omega\to\sigma\rho}$ rates calculated in Sec. II are supplied as input data for MEQO2.FOR (option 2), yielding the contribution of each elementary collision to the instantaneous rotational population rate dP_i/dt, i.e., the individual terms in the RH-side of the MEQ (13). The numerical values of $a_{\tau\omega\sigma\rho}$ coefficients and the $a_{\tau\omega\sigma\rho}k^{down}_{\tau\omega\to\sigma\rho}$ factors at different points (temperatures) of one of the O_2 jets investigated here are given in the supplementary material, columns F and H of Tables A6 to A13.[45]

The comparison of the experimental LH-side of MEQ (13) for the rotational triads $i = N = 1, 3, 5, 7$ with the corresponding experimental-calculated RH-side at different points of the supersonic jet allows the accuracy of the calculated $k^{down}_{\tau\omega\to\sigma\rho}$ rates to be assessed, providing a wealth of information about the collisional processes. The procedure is described in Sec. V in more detail.

IV. EXPERIMENT AND DATA REDUCTION

The methodology employed here[48–50] relies on the properties of supersonic free jets, and on the remarkable capabilities of Raman spectroscopy to measure accurately local quantities along a jet.[51–53] Two continuous free jets of O_2 at stagnation pressures $p_0 = 230$ and 100 mbar, and stagnation temperature $T_0 = 297$ K, have been measured. The background pressures in the vacuum chamber were 0.0015 mbar and 0.0010 mbar, respectively. These jets were generated by expanding the gas through a commercial airbrush nozzle[54] of diameter $D = 280$ μm into a $55 \times 44 \times 59$ cm^3 vaccum chamber specially devised for quantitative Raman spectroscopy. Its vacuum system is based on a 2000 liter/s turbomolecular pump backed by a 25 m^3/h scroll pump.

Raman scattering was excited with 5.5 W at 514.5 nm from an Ar^+-laser beam sharply focused perpendicular to the jet axis. The Raman signal was collected at 90° from both, the jet axis and the laser beam, and was projected with ×10 magnification onto the entrance slit of the spectrometer. This is an additive double-monochromator with gratings of 2400 l/mm equipped with a CCD detector refrigerated by liquid N_2.

The best data set has been obtained from the jet at $p_0 = 230$ mbar. Due to its higher density, compared to the 100 mbar jet, it yields Raman spectra of better signal to noise ratio. In addition, the zone of silence of the 230 mbar jet is less perturbed by the barrel shock boundary than its 100 mbar counterpart. It is well established that the width of the barrel shock boundary is inversely correlated with Reynolds numbers at the source,[55] which are $Re^* = 1172$ and $Re^* = 390$ for the 230 and 100 mbar jets, respectively. Consequently, the barrel of the 100 mbar jet is expected to be about three times broader than that of the 230 mbar jet. Actually, there is some evidence that the $z > 5000$ μm axial region of the 230 mbar jet, and the $z > 3500$ μm axial region of the 100 mbar jet are perturbed by molecules from the hot barrel at ≈290 K. This causes an undesired slight increase of the temperatures and constrains the range of accurate thermal data to $T_t \geq 10$ K and $T_t \geq 16$ K for the 230 and 100 mbar jets, respectively.

For the aforementioned reasons, the validation of the $k_{\ell m \to ij}$ rates calculated in Sec. II is based preferentially on the data from the 230 mbar jet, while the data from the 100 mbar jet show good agreement with them in the range $16 \leq T_t \leq 34$ K.

The primary experimental quantities n and P_i were determined at a number of points along the jet axis at distances z from the nozzle, as follows.

The number densities $n(z)$ were measured from the integrated Raman intensity of the Q branch of the vibrational band of $^{16}O_2$ at 1555 cm^{-1},

$$I_{1555}^{vib} = K\, n(z), \tag{14}$$

which is, to a very good approximation, proportional to the number density of O_2 molecules at the focal spot of the exciting laser beam for a wide range of conditions. The constant K was determined using static O_2 as a reference in the expansion chamber at a pressure of 22 mbar which was measured with a MKS Baratron 690A of nominal accuracy of 0.08% of reading. The space resolution of the Raman scattering experiment is high enough to avoid interferences from the lateral distribution around the paraxial region of the jet, not only for the number density, but for all other flow quantities measured.

The populations $P_i(z)$ for $i = N$ were determined from the integrated intensities $I(z)$ of the triplets associated with the $N \to N + 2$ rotational Raman transitions,[19,56] which can be reduced to

$$P_N(z) = G\, I(z)_{N \to N+2} \frac{(2N+1)(2N+3)}{(N+1)(N+2)}. \tag{15}$$

for the present purpose. The constant G is determined from the normalization condition $\sum_N P_N = 1$. Representative rotational Raman spectra recorded along the jet axis of one of the expansions are shown in Fig. 3. There, the $1 \to 3$ triplet is evident, the $3 \to 5$ triplet shows a central line and two weak satellites, and in the $5 \to 7$ and subsequent triplets only the central line is detectable under the present conditions.

While $n(z)$ and $P_i(z)$ are directly measured in the experiment, $T_r(z)$ and $T_t(z)$ are inferred from them. A first important step is to check to what extent the rotational populations $P_i(z)$ of the $i = N$ triads obey along the jet to a Boltzmann-like distribution, so that a rotational temperature $T_r(z)$ is physically meaningful. This is checked in two ways, by means of Boltzmann-plots, and then by recalculating the Boltzmann distribution of populations at different rotational temperatures and comparing them with the experimental populations. Both procedures were consistent proving unambiguously that the vast majority of the molecules are accurately represented by a rotational temperature T_r, as reported before for supersonic jets of N_2 at comparable source conditions.[43,48,57,58] Minor deviations from a Boltzmann distribution were observed just at the lower end of observable densities, consistently with an increasing collisional deficit. This fully justifies the Boltzmann distribution hypothesis employed for T_r in earlier relaxation studies, but not the T_r values reported for O_2 jets on the basis of an energy balance,[59] which are about 40% higher than the present ones for comparable source conditions. Consequently, the reported rotational collision number $Z_r \approx 2$ (Ref. 59) is too high. Present results lead to a value $Z_r \approx 1$.

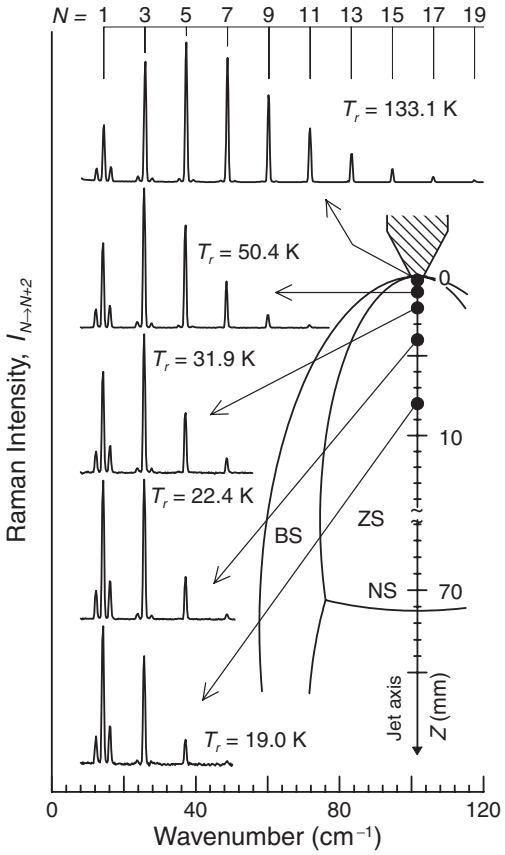

FIG. 3. Rotational Raman spectra of $^{16}O_2$ in a supersonic jet at $p_0 = 230$ mbar and $T_0 = 297$ K through a $D = 280$ μm nozzle, showing the $N \to N + 2$ triplets. ZS = zone of silence; NS = normal shock; BS = barrel shock.

In order to obtain as much information as possible from the discrete experimental data, these have been treated according to numerical procedures which allow for detection of systematic errors, smoothing, interpolation, statistical analysis of random errors, and accurate numerical derivation in the case of the populations P_i in the LH-side of Eqs. (10) and (13). The so treated experimental $n(z)$, $T_r(z)$, and $P_i(z)$ for $i = N = 1, 3, 5, 7$ of the jet at $p_0 = 230$ mbar are shown in Figs. 4, 5, and 6. The values of these quantities for the jets generated at $p_0 = 230$ and 100 mbar are given in Tables A4 and A5 of the supplementary material.[45]

The translational temperature $T_t(z)$ has been deduced from the corresponding local number density and rotational temperature, by means of

$$T_t(z) = \left(\frac{n}{n_e}\right)^{2/3} \left[T_e - \frac{2}{3}\int_{z_e}^{z} \left(\frac{n}{n_e}\right)^{-2/3} \left(\frac{dT_r}{dz}\right) dz\right], \tag{16}$$

equation derived from the conservation of energy and momentum along the axial flow line of the supersonic jet, assuming inviscid and adiabatic flow of gas of heat capacity ratio $\gamma = 7/5$.[60] Subindex e refers to any point of the jet where the breakdown of the rotational-translational thermal equilibrium is still undetectable within experimental accuracy, i.e., satisfying the condition $T_r = T_t = T_e$ for $z \leq z_e$. It must be stressed that Eq. (16) does not imply isentropic flow, as was assumed

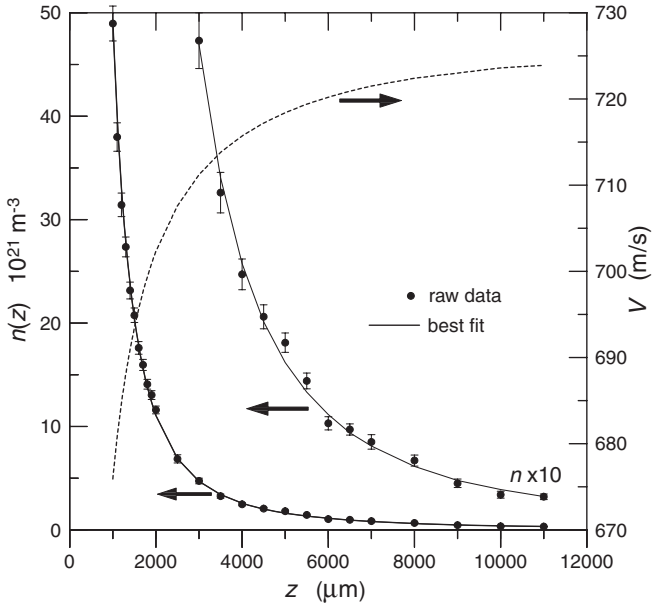

FIG. 4. Number density (raw and fit) and flow velocity along the axis of a supersonic jet of O_2 at $p_0 = 230$ mbar, $T_0 = 297$ K, through a $D = 280$ μm nozzle. Error bars are 1σ with respect to the best fit.

for the zone of silence of the jets in previous works.[43,49,50] Nonetheless, Eq. (16) yields T_t values close to those of the isentropic relation

$$T_{isen}(z) = T_0 \left(1 + \frac{\gamma - 1}{2} M^2\right)^{-1}, \tag{17}$$

in terms of the Mach number $M(z)$,[61] provided the $T_r \neq T_t$ breakdown of equilibrium at z is moderate, as is the case with the present jets. In fact, Eq. (17) is equivalent to Eq. (16) for

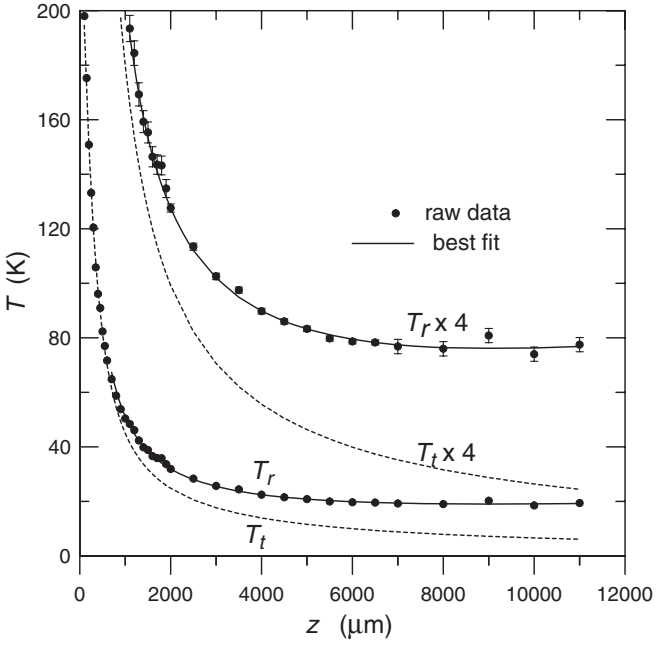

FIG. 5. Rotational (raw and fit) and translational temperatures along the axis of a supersonic jet of O_2 at $p_0 = 230$ mbar, $T_0 = 297$ K, through a $D = 280$ μm nozzle. Error bars are 1σ with respect to the best fit.

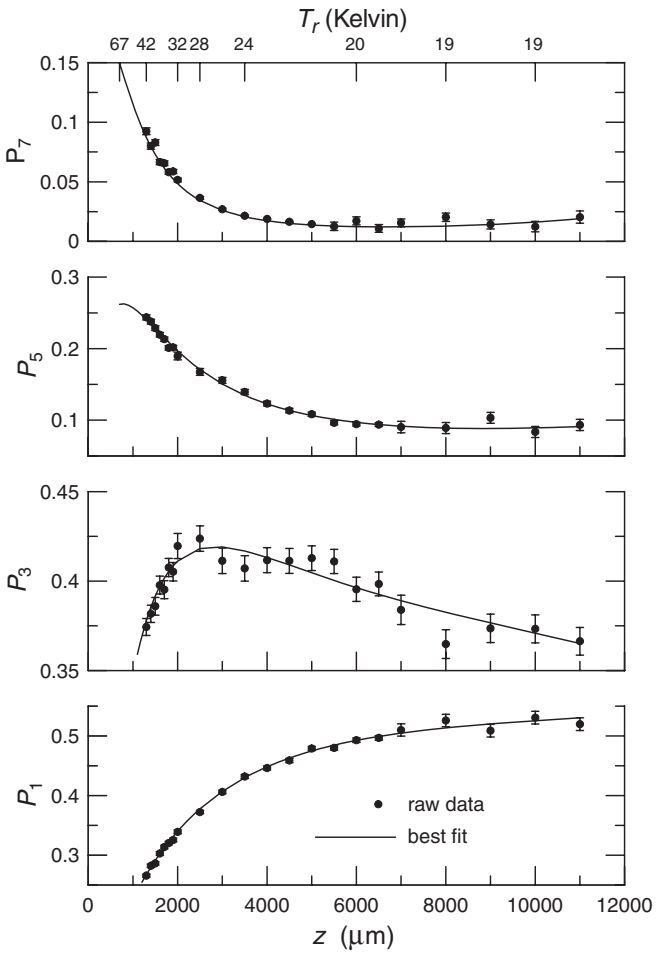

FIG. 6. Population of rotational triads $N = 1, 3, 5, 7$ (raw and fit) along the axis of a supersonic jet of O_2 at $p_0 = 230$ mbar, $T_0 = 297$ K, through a $D = 280$ μm nozzle. Error bars are 1σ with respect to the best fit.

$z \leq z_e$, and provides here an approximation better than 0.7 K for $z > z_e$.

The limits of validity of Eqs. (16) and (17) downstream in the jet are imposed by the availability of enough elastic collisions. If the number of remaining collisions from a point z_q is less than one, a progressive freezing of T_t for $z > z_q$ can be expected, Eqs. (16) and (17) becoming no longer valid.[57,58] The point z_q is estimated here on the basis of the similarity flow theory using the Reynolds number (Re^*) at the source as a similarity parameter, and the terminal translational temperatures of N_2 at the same values of Re^*.[58] The estimated terminal temperatures for the 230 and 100 mbar O_2 jets are $T_{t\infty} = 3.9$ and $T_{t\infty} = 7.4$ K, respectively. This sets the approximate limits of validity of Eqs. (16) and (17) in $z \leq 9000$ μm and $z \leq 5000$ μm, which correspond to translational temperatures $T_t \geq 7$ K for the 230 mbar jet, and $T_t \geq 12$ K for the 100 mbar jet. However, the aforementioned perturbation caused by the barrel boundary of the jets increases these limits to about 10 and 16 K, respectively.

In the explored region of the jet (zone of silence) the flow is laminar, and the distance z can be related with the time t elapsed from the beginning of the expansion ($z = 0$) by means of the flow velocity $V(z) = dz/dt$. The population rates in the

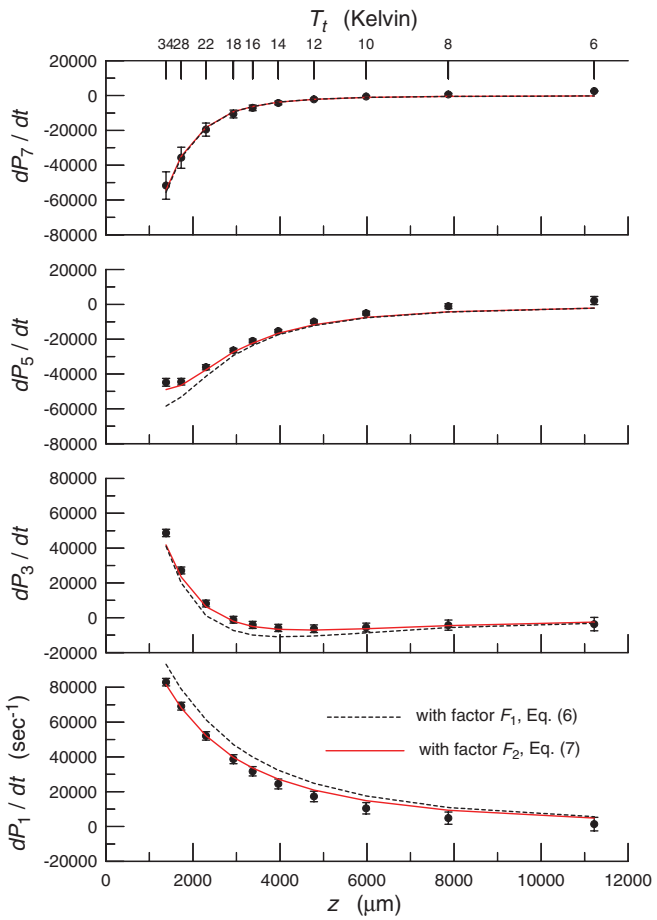

FIG. 7. RH- (lines) vs LH-side (symbols) of MEQ (13) in the supersonic jet of O_2 at $p_0 = 230$ mbar, $T_0 = 297$ K, through a $D = 280$ μm nozzle (see text). Error bars of experimental LH-side are 1σ.

LH-side of MEQ (13) are thus determined from

$$\frac{dP_i}{dt} = \frac{dP_i}{dz} V(z). \tag{18}$$

Accurate values for the gradients dP_i/dz were retrieved from the smoothed rotational populations $P_i(z)$ (see Table A5 in[45]), while the flow velocity $V(z)$ in Eq. (18) was determined assuming the conservation of energy along the jet axis,[60] which leads to

$$V(z) = [R(7T_0 - 5T_t(z) - 2T_r(z))/W]^{1/2}, \tag{19}$$

with $R = 8.3145$ J K^{-1} mol^{-1} for the universal gas constant and $W = 0.032$ kg/mol for the molar mass of $^{16}O_2$. Flow velocities shown in Fig. 4 are listed in Table A4.[45]

V. DISCUSSION

The calculated rates (Table I and Table A3 of supplementary material[45]) have been assessed experimentally for $10 \le T_t \le 34$ K by their capability to reproduce the measured dP_i/dt-values of MEQ (13) along the jet as a function of the translational temperature T_t. The LH- versus RH-sides comparison of MEQ (13) is done at fixed points with translational temperatures $T_t = 34, 28, 22, 18, 16, 14, 12, 10$ K, and is shown in Fig. 7 and in Table II. They prove an outstanding agreement, free from any fitting parameter, between a first principles quantum calculation and an experiment where flow dynamic quantities vary by orders of magnitude for a large data set.

TABLE II. Comparison of the LH- versus RH-side of the MEQ (13) along a supersonic jet of O_2 generated at $p_0 = 230$ mbar, $T_0 = 297$ K, through a $D = 280$ μm nozzle; dP_i/dt in units of 10^2 s^{-1}. Uncertainty of the LH-side is 1σ. For uncertainty of the RH-side, see text.

T_t/K		dP_1/dt	dP_3/dt	dP_5/dt	dP_7/dt
34	LH	829 ± 22	487 ± 21	-448 ± 22	-517 ± 79
	RH	814 ± 22	418 ± 69	-490 ± 42	-543 ± 79
28	LH	691 ± 23	271 ± 20	-444 ± 19	-357 ± 60
	RH	682 ± 23	234 ± 37	-465 ± 21	-350 ± 60
22	LH	521 ± 24	82 ± 19	-361 ± 15	-196 ± 37
	RH	522 ± 24	64 ± 19	-376 ± 15	-184 ± 37
18	LH	387 ± 26	-11 ± 19	-265 ± 12	-106 ± 22
	RH	398 ± 26	-20 ± 19	-274 ± 12	-93 ± 22
16	LH	317 ± 27	-41 ± 20	-210 ± 11	-71 ± 16
	RH	337 ± 27	-50 ± 20	-223 ± 13	-63 ± 16
14	LH	245 ± 28	-59 ± 21	-154 ± 10	-43 ± 11
	RH	272 ± 28	-66 ± 21	-166 ± 12	-38 ± 11
12	LH	173 ± 30	-63 ± 22	-100 ± 10	-21 ± 7
	RH	209 ± 36	-71 ± 22	-117 ± 17	-21 ± 7
10	LH	105 ± 32	-56 ± 25	-51 ± 11	-6 ± 4
	RH	149 ± 44	-63 ± 25	-75 ± 24	-11 ± 5

The uncertainty quoted in Table II for the LH-side of MEQ (13) is the experimental one (1σ) as propagated from that of P_i. The uncertainty for the RH-side deserves some comments in the frame of the Monte Carlo procedure employed to estimate the confidence intervals of the calculated rates. It was set as follows: If the calculated RH-value matches the LH-value within its experimental uncertainty, this is taken as the reference uncertainty. Else, the uncertainty of the RH-value is taken as the difference between experiment and calculation as given in Table II.

A detailed insight of what is going on in the jet from the point of view of the collisional energy transfer can be inferred from the Tables A6–A13.[45] There, the contribution of the individual $k_{ij\to\ell m}$ rates to the RH-side of MEQ (13) is given explicitly. Tables A6–A13 can be easily converted to linear equations which provide the basis for an objective estimate of the confidence interval of the calculated rates. This is done by Monte Carlo simulation randomly generating 1000 sets of rates with a normal distribution centered at the values calculated in Sec. II (Table I and Table A3 of auxiliary material[45]), and standard deviation to be determined until overlapping with the experimental values of the LH-side of MEQ (13) given in Table II is attained. This way one assures that the confidence interval obtained for the rates is statistically consistent with the experiment.

The result of the procedure described above is summarized in Table I. At $T_t = 34$ K some rates are determined to ≈6% ($k_{33\to13}, k_{53\to13}$), some others to ≈10% ($k_{31\to11}, k_{51\to31}, k_{53\to33}$), and the remaining ones show larger uncertainties. As can be seen in the sample of Table I, the confidence interval gets wider with decreasing temperatures, many of the rates at $T_t = 10$ K becoming ill-determined by

the experiment. This is due in part to the degraded accuracy of the experimental data in the terminal distance of the experiment, and intrinsically to the low population of the rotational triads other than $N = 1$ (see Fig. 6), causing the coefficients $a_{\tau\omega\sigma\rho}$ to become very small and the products $a_{\tau\omega\sigma\rho} \times k^{down}_{\tau\omega\to\sigma\rho}$ negligible. Note also that the dP_i/dt's from Fig. 7 and Table II tend asymptotically to zero for decreasing temperatures, the trend being more pronounced for higher values of $i = N$. This indicates that the quality of the information on the rates is not homogeneous along the jet. As a rule, the relative uncertainty of dP_i/dt's is small at short distances from the nozzle ($z = 1380$ μm, $T_t = 34$ K), and large at the longer distances ($z = 7870$ μm, $T_t = 8$ K).

Further comments on the confidence intervals of the rates are pertinent. Every $k_{ij\to\ell m}$ rate associated to an inelastic collision implies at least two rotational N-triads. For instance, $k_{33\to31}$ accounts for the collisional depletion of the $N = 3$ triad of O_2, and the simultaneous population of the $N = 1$ triad. Other rates like $k_{51\to33}$ involve three triads, depleting the $N = 5$ and $N = 1$ triads, and populating $N = 3$. Others like $k_{17\to35}$ involve four triads. This means that these rates appear in the dP_1/dt and dP_3/dt terms of the MEQ (13) in the first case, in the dP_1/dt, dP_5/dt, and dP_3/dt terms in the second case, and in the dP_1/dt, dP_7/dt, dP_5/dt, and dP_3/dt terms in the last case. In other words, this provides double, triple, or fourfold experimental information on a given rate, with different levels of quality depending on the "noise" of the experimental data points concerning the rotational populations measured. As can be inferred from Figs. 6 and 7 and from Tables A6 to A13,[45] the confidence interval for every $k_{ij\to\ell m}$ rate has an optimum corresponding to the best determined value of the dP/dt's involved. This "best confidence interval" is the one listed in Table I and in the more complete Table A3.[45]

The controversial factor F_α in Eq. (8) can be discussed in the light of the experimental results. The dashed lines in Fig. 7 correspond to the calculated cross sections and rates employing the factor F_1 defined by Eq. (6), and the solid lines to the factor F_2 defined by Eq. (7). Figure 7 shows that the factor F_1 leads to results far less consistent with the experiment than factor F_2, which we judge the correct one on the basis of statistical arguments. Moreover, when interpreted in terms of confidence intervals according to the procedure outlined above, the confidence intervals with F_1 become about five times broader than with F_2, i.e., showing a far larger uncertainty for the calculated rates. This happens not only for the $k_{ii\to\ell\ell}$ rates affected by F_α but for the whole set of rates, many of them becoming ill-determined.

Let us close this study by showing the remarkable similarities found between the calculated rates of two diatomic molecules which have been treated in the common theoretical frame of the close-coupling method. These collisional systems are the present O_2:O_2 and the previously studied N_2:N_2,[43] whose para-N_2 variant is homologous to O_2. Although the validation of rates from the previous study of N_2:N_2 collisions was not as successful as for O_2:O_2, it is instructive to compare the calculated rates of both systems. This is shown in Table III, at $T_t = 22$ K, where the average ratio $\langle R\rangle(N_2/O_2) = 1.26 \pm 0.12$ is obtained for rate values and energy gaps varying by a factor up to ≈30. This suggests that the anisotropy of the PES's (Ref. 31 and 62) employed for calculating the rates of both systems is not too different, a point which deserves a closer scrutiny in future works. On the other hand, just a crude correlation between the rates and their reduced energy gaps Δ/B is observed, with decreasing rates for increasing Δ/B, indicating that the longly pursued scaling laws are more complex than expected.

TABLE III. Comparison of calculated down-rates for O_2:O_2 and pN_2:pN_2 inelastic collisions at $T_t = 22$ K. Rates are in units of 10^{-20} m^3 s^{-1}. Colliding molecules are considered indistinguishable.

Process	Δ/B	O_2:O_2 rate[a]	pN_2:pN_2 rate[b]	$R(N_2/O_2)$
$55 \to 17$	2	1348	1784	1.323
$51 \to 33$	8	5351	7310	1.366
$31 \to 11$	10	3621	4738	1.308
$33 \to 13$	10	4060	5237	1.290
$35 \to 15$	10	4728	6088	1.288
$17 \to 35$	16	6364	7480	1.175
$51 \to 31$	18	5475	6821	1.246
$53 \to 33$	18	3941	4840	1.228
$55 \to 35$	18	3544	4211	1.188
$33 \to 11$[c]	20	806	1090	1.352
$71 \to 51$	26	3845	4015	1.044
$51 \to 11$	28	1132	1429	1.262
$53 \to 13$	28	2948	4053	1.375
$55 \to 15$	28	1242	1693	1.363
$71 \to 33$	34	1831	2283	1.247
$55 \to 33$[c]	36	1034	1077	1.042
$53 \to 11$	38	531	799	1.505
$71 \to 31$	44	2121	2370	1.117
$55 \to 31$	46	727	886	1.219
$71 \to 11$	54	521	576	1.105
$55 \to 11$[c]	56	157	228	1.452
				$\langle R\rangle = 1.26 \pm 0.12$

[a]This work;
[b]Reference 43.
[c]Calculated with factor F_2.

VI. SUMMARY, FUTURE PROSPECTS, AND CONCLUSIONS

Close-coupling calculations for O_2:O_2 inelastic collisions have been performed using the fully *ab-initio* singlet, triplet, and quintet PES's of Ref. 31. State-to-state cross sections have been calculated for 66 inelastic $ij \to \ell m$ collisional processes involving rotational triads of O_2 up to $N = 9$, in a grid of energies up to 300 cm^{-1}. The three sets of cross sections have been averaged over their spin multiplicities and transformed into the corresponding state-to-state rate coefficients for the temperature range $4 \le T_t \le 34$ K. The accuracy of these rates has been assessed experimentally in the range $10 \le T_t \le 34$ K by means of the Master Equation describing the evolution of rotational populations along the jet as measured by Raman spectroscopy. The 1σ confidence interval estimated for the rates on the basis of the experimental data rests upon a Monte Carlo procedure.

This confidence interval varies very much with the translational temperature and with the particular rate coefficient.

As a rule the confidence interval at low temperature is broader, and rates involving higher N-triads have, in general, larger uncertainties. Among the 66 rates, the best determined ones by the experiment are accurate (1σ) to $\approx$6% in the higher end of translational temperatures investigated, $T_t = 34$ K. In the lower end accessible to the experiment with confidence, $T_t = 10$ K, the best determined rates are accurate to 17%. All rates show a smooth dependence on the translational temperature in the range $4 \leq T_t \leq 34$ K.

From the experimental point of view these results are amenable to improvement, i.e., narrowing the confidence intervals of the rates by optimizing the design of the experiment. In particular, the study of O_2 jets with the same nozzle at higher stagnation pressures, up to 1 bar, would reduce substantially the spectral noise, improving the accuracy of the measured flow quantities. Under these conditions, a better sampling of the datapoints along the jet would surely allow reaching $T_t \approx 6$K. Stagnation pressures higher than 1 bar may induce some condensation, introducing systematic errors. A survey jet of O_2 expanded at $p_0 = 10$ bar through a $D = 90$ μm nozzle has shown clear evidence of condensation at $z \geq 5D$. The released condensation heat[60] increases the temperature and cannot be quantified with the accuracy required by the present methodology. On the other hand, significant cooling of the nozzle in order to reach lower temperatures would also lead to the undesired effect of condensation.

A point which needs to be considered carefully for future experiments is the characterization of the rotational temperature profile across the barrel boundary of the jet. As observed here, at downstream distances $z/D > 15$ the barrel tends to contaminate thermally the paraxial region of the jet rising its temperature, specially for low Reynolds numbers ($Re^* < 500$) at the source. Removal of this thermal contamination would probably extend the experimentally accessible range down to $T_t \approx 4$ K.

Translational temperatures up to 60 K can be reached in the experiment easily, and even higher by employing slit nozzles, but the Master Equation should require a set of rates much larger than that obtained here. This is indeed a problem of computational cost where alternative approaches as the coupled-states approximation[63] might prove useful for the present experimental method at higher temperatures.

An interesting problem closely related to the present work is the possibility of studying collisional quasi-elastic processes occurring within a given N-triad of O_2, like

$$O_2(N, J_a) + O_2(N, J_b) \longrightarrow O_2(N, J'_a) + O_2(N, J'_b). \tag{20}$$

Quantum calculations of cross sections for these processes have been reported at zero-[64] and non-zero magnetic field[65,66] for the ultracold regime. Due to the much higher energy regime considered in the present work only a coarse comparison with the zero-field case is possible. The calculated inelastic cross sections[64] within the $N = 1$ triad of $^{16}O_2$ show peak values ranging from 10 to 100 Å^2 located at energies between 0.1 and 1 K, i.e., somewhat smaller than the largest down cross sections calculated here for inter-triad collisions.

Within the present experimental methodology the study of $N = 1$ quasi-elastic collisions does not seem possible for O_2:O_2, due to the low rotational temperatures required, well under 4 K. However, since rotational temperatures below this threshold are easier to attain in $O_2 + He$ mixed jets, a simpler variant of this problem seems feasible for O_2:He.[25–28] An open question worth to be investigated is whether the alignment of O_2 in $O_2 + He$ jets[67] can be detected and quantified by the present methodology.

In addition to the quantitative results reported here, the following general conclusions are drawn:

(1) The present computational results (Table A3 in Ref. 45) and the experimental jet data (Tables A4 and A5 in Ref. 45) provide a solid basis for the interpretation of relaxation phenomena in low-temperature O_2 in terms of elementary collisional processes, since some transport coefficients, such as the volume viscosity, rotational relaxation cross section, relaxation time, collision number and, in part, the thermal conductivity depend on the inelastic state-to-state cross sections or rates.[3–11] Although not in the scope of present work, earlier modeling of supersonic jets and related concepts[59] can be re-examined in the light of far more accurate data. In addition, the rates are a fundamental part of spectral line broadening, shifting, and mixing coefficients for remote sensing applications involving O_2.[1]

(2) The calculated rates prove consistent with the experiment to better than 10% in the favourable cases. This strongly suggests that the anisotropy of the fully *ab-initio* PES's employed in the calculation[31] is of very good quality in the range of collisional energies up to 300 cm^{-1}, and that the Hamiltonian employed for the nuclei dynamics is highly reliable.

(3) The theoretical-experimental methodology combining as a whole close-coupling calculations, supersonic jets, Raman spectroscopy, Master Equation, and Monte Carlo sampling, proves highly efficient for obtaining and assessing state-to-state rate coefficients of molecular gases at temperatures well below their freezing point, a region hardly accessible to other techniques based on static gas samples. This is important for the study of sharp non-equilibrium problems in astrophysics, in particular, cold collisions of relevant molecules of the interstellar medium (H_2O, CO) with far more abundant light projectiles (H_2, He).

(4) Finally, the unifying character of the present work should be stressed, as it successfully merges concepts and equations from the molecular quantum world (Schrödinger equation, Master Equation) with macroscopic quantities from fluid mechanics (in Boltzmann and Navier-Stokes equations) which vary by orders of magnitude in the time scale of μs. The full agreement of theory with experiment found here, paves the way for a complete understanding of the multiple facets of non-equilibrium gas dynamics.

ACKNOWLEDGMENTS

This work has been supported by the Spanish Ministerio de Ciencia e Innovación, research projects CTQ2007-62898-BQU, FIS2007-61430, and CSD2009-00038. J.P.-R. was supported by a predoctoral JAE-CSIC grant. We wish to thank M. Bartolomei, E. Carmona-Novillo, J. Campos-Martínez, and R. Hernández-Lamoneda for the use of the PES prior to publication, and specially to J. Campos-Martínez for very

valuable suggestions regarding the close-coupling calculations.

[1]J. M. Hartmann, C. Boulet, and D. Robert, *Collisional Effects on Molecular Spectra: Laboratory Experiments and Models, Consequences for Appications* (Elsevier, Amsterdam, 2008).
[2]S. Green, J. Chem. Phys. **62**, 2271 (1975).
[3]C. S. Wang-Chang and G. E. Uhlenbeck, University of Michigan Report No. CM-681, 1951.
[4]C. S. Wang-Chang, G. E. Uhlenbeck and J. de Boer, in *Studies in Statistical Mechanics*, edited by J. de Boer and G. E. Uhlenbeck (North Holland, Amsterdam, 1964), Vol. 2, pp. 241–268.
[5]L. Waldmann, in *Handbuch der Physik*, edited by S. Flügge (Springer-Verlag, Berlin, 1958), Vol. XII, pp. 295–514.
[6]R. F. Snider, Int. Rev. Phys. Chem. **17**, 185 (1998).
[7]E. A. Mason and L. Monchick, J. Chem. Phys. **36**, 1622 (1962).
[8]W. E. Köhler and J. Schaefer, J. Chem. Phys. **78**, 4862 (1983); J. Chem. Phys. **78**, 6602 (1983).
[9]F. R. W. McCourt, J. J. M. Beenakker, W. E. Köhler, and I. Kuscer, *Nonequilibrium Phenomena in Polyatomic Gases* (Clarendon, Oxford, 1991).
[10]C. Nyeland, in *Molecular Physics and Hypersonic Flows*, NATO ASI Series C: Mathematical and Physical Sciences, Vol. 482, edited by M. Capitelli (Kluwer Academic Publishers, Doordrecht, 1996), pp. 393–404.
[11]L. Wang and G. D. Billing, J. Phys. Chem. **97**, 2523 (1993).
[12]U. Mingelgrin and R. G. Gordon, J. Chem. Phys. **70**, 3828 (1979).
[13]A.-Predoi-Cross, K. Harnbrook, R. Keller, C. Povey, I. Schofield, D. Hurtmans, H. Over, and G. C. Mellau, J. Mol. Spectrosc. **248**, 85 (2008).
[14]M. Y. Tretyakov, M. A. Koshelev, V. V. Dorovskikh, and D. S. Makarov, J. Mol. Spectrosc. **231**, 1 (2005).
[15]D. S. Makarov, I. A. Koval, M. A. Koshelev, V. V. Parshin, and M. Y. Tretyavov, J. Mol. Spectrosc. **252**, 242 (2008).
[16]Y. Ouazzany, J. P. Boquillon, and B. Lavorel, Can. J. Phys. **65**, 1588 (1987).
[17]G. Millot, R. Saint-Loup, J. Santos, R. Chaux, and H. Berger, J. Chem. Phys. **96**, 961 (1992).
[18]G. Millot, B. Lavorel, and G. Fanjoux, J. Mol. Spectrosc. **176**, 211 (1996).
[19]M. Bérard, P. Lallemand, J. P. Cebe, and M. Giraud, J. Chem. Phys. **78**, 672 (1983).
[20]K. S. Lam, J. Quant. Spectrosc. Radiat. Transf. **17**, 351 (1977).
[21]P. W. Rosenkranz, J. Quant. Spectrosc. Radiat. Transf. **39**, 287 (1988).
[22]H. J. Liebe, P. W. Rosenkranz, and G. A. Hufford, J. Quant. Spectrosc. Radiat. Transf. **48**, 629 (1992).
[23]V. Aquilanti, D. Ascenzi, M. Bartolomei, D. Cappelletti, S. Cavalli, M. de Castro Vitores, and F. Pirani, Phys. Rev. Lett. **82**, 69 (1999).
[24]V. Aquilanti, D. Ascenzi, M. Bartolomei, D. Cappelletti, S. Cavalli, M. de Castro Vitores, and F. Pirani, J. Am. Chem. Soc. **121**, 10794 (1999).
[25]P. Maréchal, Y. P. Viala, and J. J. Benayoun, Astron. Astrophys. **324**, 221 (1997).
[26]N. Balakrishnan and A. Dalgarno, J. Phys. Chem. A **105**, 2348 (2001).
[27]F. Lique, J. Chem. Phys. **132**, 044311 (2010).
[28]G. C. Corey, M. H. Alexander, and J. Schaefer, J. Chem. Phys. **85**, 2726 (1986).
[29]J. Pérez-Ríos, M. Bartolomei, J. Campos-Martínez, M. I. Hernández, and R. Hernández-Lamoneda, J. Phys. Chem. A **113**, 14952 (2009).
[30]MOLSCAT, Collaborative Computational Project nº6 of the UK Science and Egineering Research Council, designed by J. M. Hutson and S. Green, version 14 (1994).
[31]M. Bartolomei, E. Carmona-Novillo, M. I. Hernández, J. Campos-Martínez, and R. Hernández-Lamoneda, J. Chem. Phys. **133**, 124311 (2010).
[32]P. E. S. Wormer and A. van der Avoird, J. Chem. Phys. **81**, 1929 (1984).
[33]B. Bussery and P. E. S. Wormer, J. Chem. Phys. **99**, 1230 (1993).
[34]M. Bartolomei, E. Carmona-Novillo, M. I. Hernández, J. Campos-Martínez, and R. Hernández-Lamoneda, J. Chem. Phys. **128**, 214304 (2008).
[35]M. Bartolomei, E. Carmona-Novillo, M. I. Hernández, J. Campos-Martínez, and R. Hernández-Lamoneda, J. Comput. Chem. **32**, 279 (2011).
[36]A. van der Avoird and G. Brocks, J. Chem. Phys. **87**, 5346 (1987).
[37]K. Takayanagi, Adv. At. Mol. Phys. **1**, 149 (1965).
[38]G. L. Zarur and Y. Chiu, J. Chem. Phys. **56**, 3278 (1972).
[39]For consistency with a Master Equation approach for distinguishable molecules, we prefer the notation $\sigma^{e}_{ij\to m\ell}$ for the exchange term, instead of $\sigma^{e}_{ij\to \ell m}$ employed by Huo and Green in Ref. 42.
[40]H. Rabitz and S. Lam, J. Chem. Phys. **63**, 3532 (1975).
[41]G. Danby, D. R. Flower, and T. S. Monteiro, Mon. Not. R. Astron. Soc. **226**, 739 (1987).
[42]W. M. Huo and S. Green, J. Chem. Phys. **104**, 7572 (1996).
[43]J. P. Fonfría, A. Ramos, F. Thibault, G. Tejeda, J. M. Fernández, and S. Montero, J. Chem. Phys. **127**, 134305 (2007).
[44]T.-G. Lee, N. Balakrishnan, R. C. Forrey, P. C. Stancil, G. Shaw, D. R. Schultz, and G. J. Ferland, Astrophys. J. **689**, 1105 (2008).
[45]See supplementary material at http://dx.doi.org/10.1063/1.3585978 for the file O2_MatAux.zip with auxiliary material of this work described in the text.
[46]M. H. Alexander and D. E. Manolopoulos, J. Chem. Phys. **86**, 2044 (1987).
[47]G. Y. Golubiatnikov and A. F. Krupnov, J. Mol. Spectrosc. **225**, 222 (2004).
[48]A. Ramos, G. Tejeda, J. M. Fernández, and S. Montero, Phys. Rev. A **66**, 022702 (2002).
[49]B. Maté, F. Thibault, G. Tejeda, J. M. Fernández, and S. Montero, J. Chem. Phys. **122**, 064313 (2005).
[50]S. Montero, F. Thibault, G. Tejeda, and J. M. Fernández, J. Chem. Phys. **125**, 124301 (2006).
[51]G. Tejeda, B. Maté, J. M. Fernández-Sánchez, and S. Montero, Phys. Rev. Lett. **76**, 34 (1996).
[52]A. Ramos, B. Maté, G. Tejeda, J. M. Fernández, and S. Montero, Phys. Rev. E **62**, 4940 (2000).
[53]S. Montero, B. Maté, G. Tejeda, J. M. Fernández, and A. Ramos, in *Atomic and Molecular Beams: The State of the Art 2000*, edited by R. Campargue (Springer, Berlin, 2001), p. 295.
[54]An atomizer for applying by compressed air a fine spray, as paint or liquid color.
[55]H. Ashkenas and F. S. Sherman, in *Proceedings of the 4th International Symposium on Rarefied Gas Dynamics*, edited by J. H. de Leeuw (Academic, New York, 1966), p. 84, Vol II.
[56]K. Altmann, G. Strey, J. G. Hochenbleicher, and J. Brandmüller, Z. Naturforsch. **27a**, 56 (1972).
[57]L. K. Randeniya and M. A. Smith, J. Chem. Phys. **93**, 661 (1990).
[58]F. J. Aoiz, T. Díez-Rojo, V. J. Herrero, B. Martínez-Haya, M. Menéndez, P. Quintana, L. Ramonat, I. Tanarro, and E. Verdasco, J. Phys. Chem. A **103**, 823 (1999).
[59]R. J. Gallagher and J. B. Fenn, J. Chem. Phys. **60**, 3487 (1974).
[60]B. Maté, G. Tejeda, and S. Montero, J. Chem. Phys. **108**, 2676 (1998).
[61]D. R. Miller, in *Atomic and Molecular Beams Methods*, edited by G. Scoles (Oxford University Press, New York, 1988), Vol. I, pp. 14–53.
[62]D. Cappelletti, F. Vechiocattivi, F. Pirani, E. L. Heck, and A. S. Dickinson, Mol. Phys. **93**, 485 (1998).
[63]S. Green, J. Boissoles, and C. Boulet, J. Quant. Spectrosc. Radiat. Transf. **39**, 33 (1988).
[64]A. V. Avdeenkov and J. L. Bohn, Phys. Rev. A **64**, 052703 (2001).
[65]T. V. Tscherbul, Yu. V. Suleimanov, V. Aquilanti, and R. V. Krems, New J. Phys. **11**, 055021 (2009).
[66]J. Pérez-Ríos, J. Campos-Martínez, and M. I. Hernández, J. Chem. Phys. **134**, 124310 (2011).
[67]V. Aquilanti, D. Ascenzi, M. de Castro Vitores, F. Pirani, and D. Cappelletti, J. Chem. Phys. **111**, 2620 (1999).